

# Pulsed EPR Dipolar Spectroscopy at Q- and G-band on a Trityl Biradical

## Supplementary Information

D. Akhmetzyanov,<sup>‡*a*</sup> P. Schöps,<sup>‡*a*</sup> A. Marko,<sup>*a*</sup> N. C. Kunjir,<sup>*b*</sup> S. Th. Sigurdsson<sup>*\*b*</sup> and  
T. F. Prisner<sup>*\*a*</sup>

<sup>*a*</sup> Goethe-University Frankfurt am Main, Institute of Physical and Theoretical Chemistry and Center for Biomolecular Magnetic Resonance, Max von Laue Str. 7, 60438 Frankfurt am Main, Germany.

E-mail: prisner@chemie.uni-frankfurt.de

<sup>*b*</sup> University of Iceland, Department of Chemistry, Science Institute, Dunhaga 3, 107 Reykjavík, Iceland.

E-mail: snorrisi@hi.is

‡ Authors contributed equally to the work

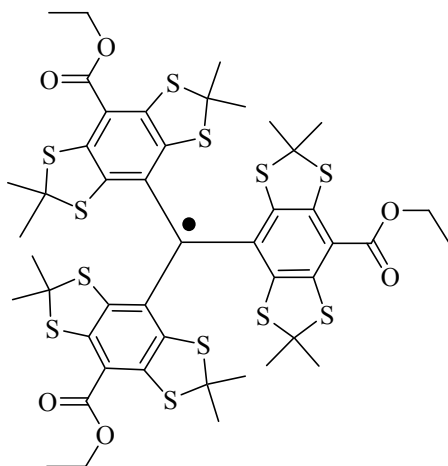
\* Corresponding authors

## Table of contents

1. Chemical structure of trityl monoradical <b>2</b> .....	3
2. G-band EPR spectrum of monoradical <b>2</b> .....	4
3. Comparison of G-band EPR spectra of <b>1</b> and <b>2</b> .....	5
4. Raw Q-band SIFTER and DQC time traces with the corresponding background functions .....	6
5. G-band PELDOR experimental data and corresponding background functions .....	7
6. Fitting of the G-band PELDOR time traces using the PELDOR database .....	8
7. References .....	13

## 1. Chemical structure of trityl monoradical **2**

Chemical structure of trityl monoradical is presented in Fig. S1. Synthesis of the monoradical is described elsewhere.<sup>1</sup>



**2**

**Fig. S1.** Chemical structure of trityl monoradical **2**.

## 2. G-band EPR spectrum of monoradical **2**

The field-swept Hahn echo-detected G-band EPR spectrum of monoradical **2** and the simulated spectrum, obtained with EasySpin software,<sup>S1</sup> are depicted in Fig. S2.

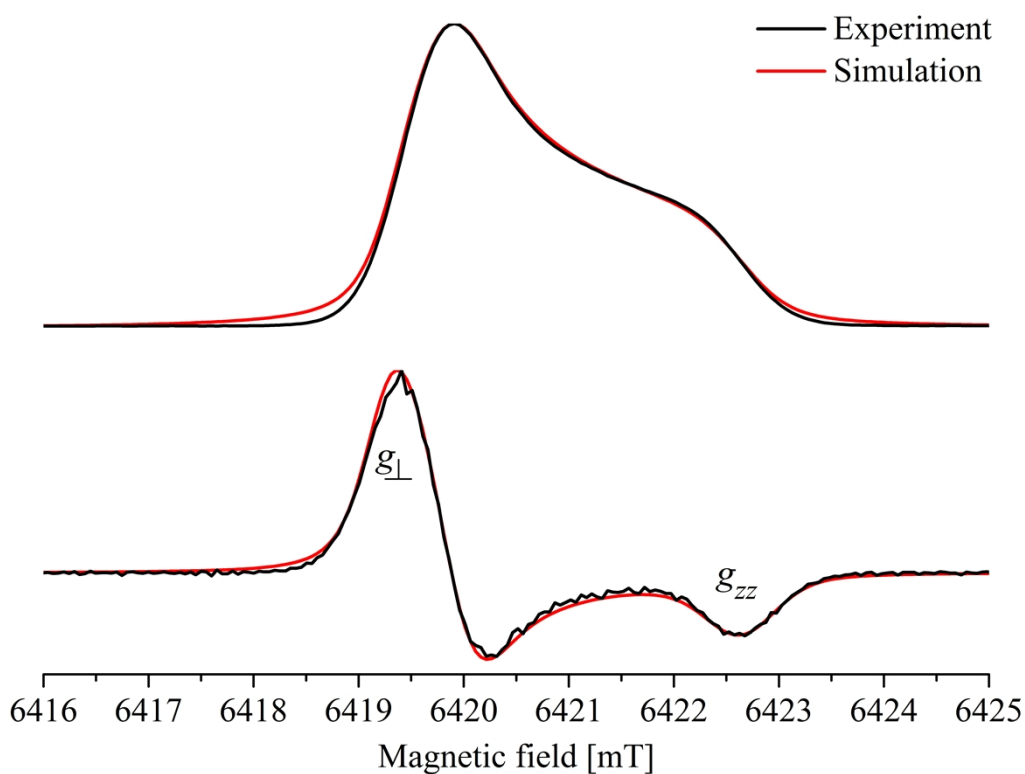


**Fig. S2. Top.** Field-swept Hahn echo-detected EPR spectrum obtained at G-band frequencies on monoradical **2** (black curve) with corresponding simulated spectrum (red curve) obtained with EasySpin. The temperature of the sample was 100 K. The concentration was 200  $\mu\text{M}$  in toluene solvent. The field was calibrated with  $\text{Mn}^{2+}$  doped MgO standard sample.

**Bottom.** Numerical differentiation of the experimental (black curve) and simulated (red curve) EPR spectra.

Parameters used for the simulation are represented in Table S1.

**Table S1.** Parameters of the EasySpin simulation

g-values			lwpp, mT		HStrain, MHz			A*,MHz		
$g_{xx}$	$g_{yy}$	$g_{zz}$	Gauss	Lorentz	x	y	z	Axx	Ayy	Azz
2.0034(1)	2.0032(4)	2.0023(7)	0.2	0.2	10	12	16	20.6	20.6	160.1

\*Principal values of the central  $^{13}\text{C}$  hyperfine coupling tensor are obtained from another study.<sup>S2</sup>

### 3. Comparison of G-band EPR spectra of **1** and **2**

The field-swept Hahn echo-detected EPR spectra of trityl mono- and biradical obtained at G-band frequencies are depicted in Fig. S3.

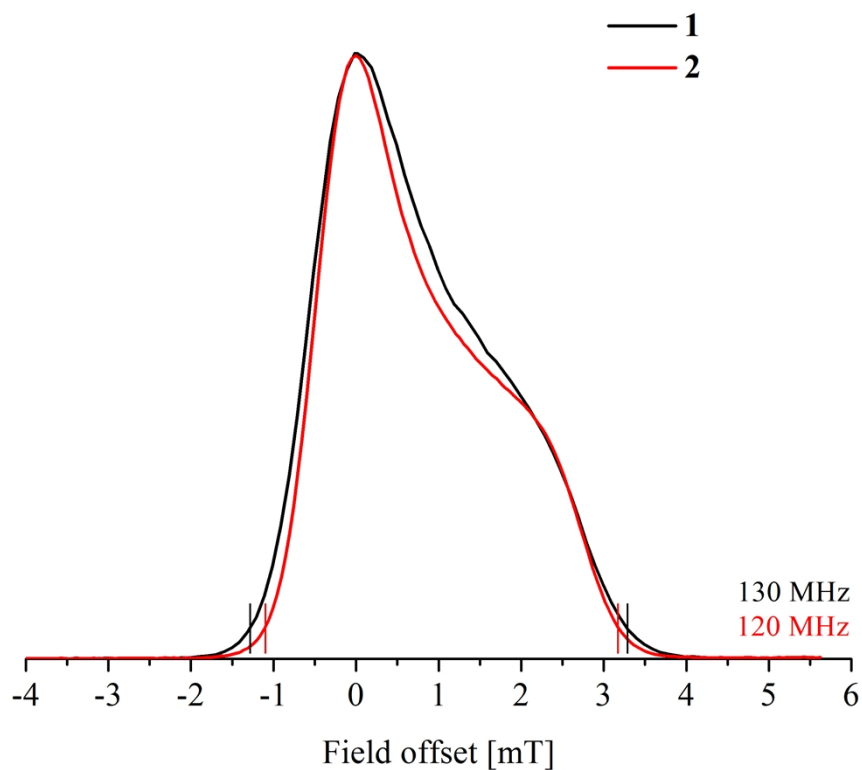


**Fig. S3.** Field-sweep Hahn echo-detected G-band EPR spectra of trityl mono- and biradical. The EPR spectrum of biradical **1** is obtained at 25 K with a concentration of 200  $\mu\text{M}$  in toluene- $d_8$  solvent. The EPR spectrum of monoradical **2** is obtained at 100 K with a concentration of 200  $\mu\text{M}$  in toluene solvent. The axis of abscissas represents the field offset from the maximum absorption position in the spectra. The field for the EPR spectrum of biradical **1** was not calibrated. The field for the EPR spectrum of monoradical **2** was calibrated with  $\text{Mn}^{2+}$  doped MgO standard sample. Parallel bars indicate the boundaries that define the width of the EPR spectra of the trityl mono- and biradical (5 % of echo intensity).

#### 4. Raw Q-band SIFTER and DQC time traces with the corresponding background functions

The Q-band SIFTER and DQC raw time traces of biradical **1** with the corresponding background functions are depicted in Fig. S4.

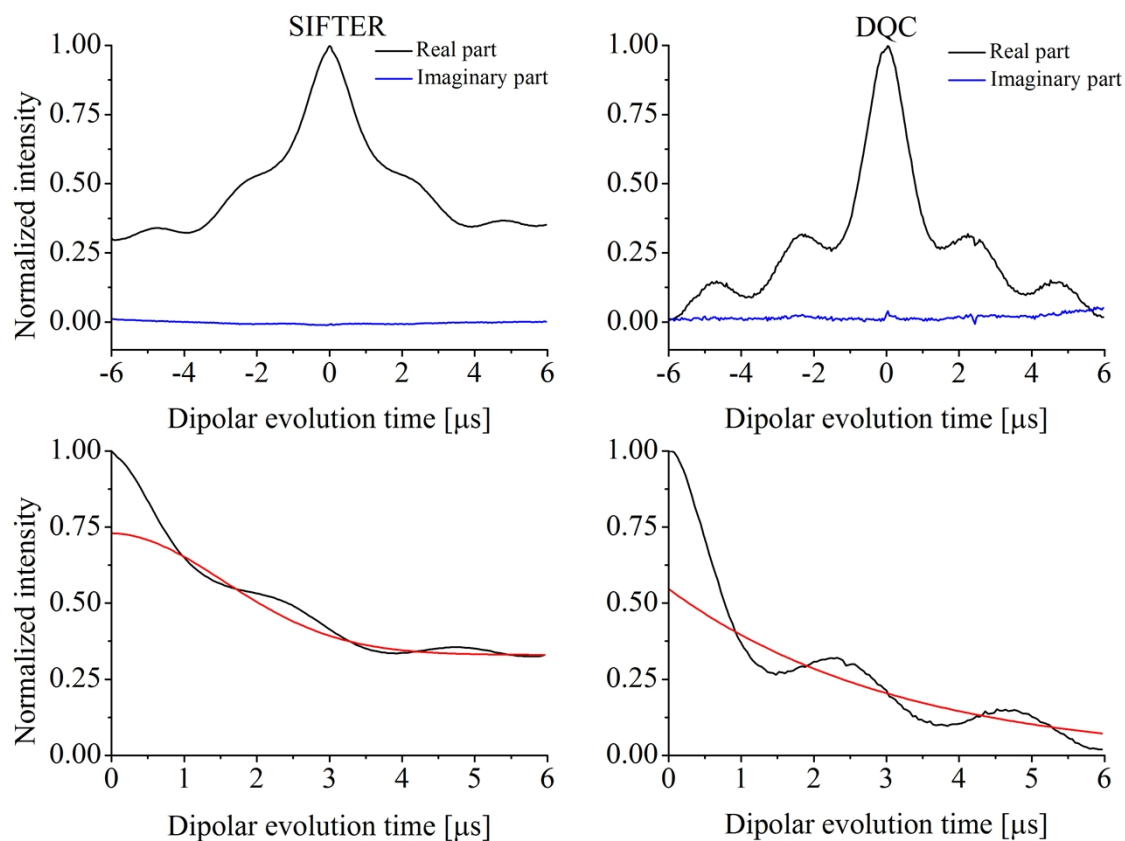


**Fig. S4. Top.** SIFTER (left) and DQC (right) raw experimental time traces obtained at Q-band frequencies at a temperature of 50 K.

**Bottom.** Black curves are the raw time traces obtained as a sum of the part of the time trace with the positive dipolar evolution time and the mirror symmetric part of the time trace with negative dipolar evolution time. Red curves are the background functions. For the SIFTER time trace the background function is obtained by a Gaussian fit of the SIFTER time trace of monoradical **2**. For the DQC time trace the background function is obtained by an exponential fit of the time trace using the EasySpin `exponfit` function.

## 5. G-band PELDOR experimental data and corresponding background functions

The experimental G-band PELDOR time traces obtained on biradical **1** are depicted in Fig. S5 with the corresponding exponential background functions.

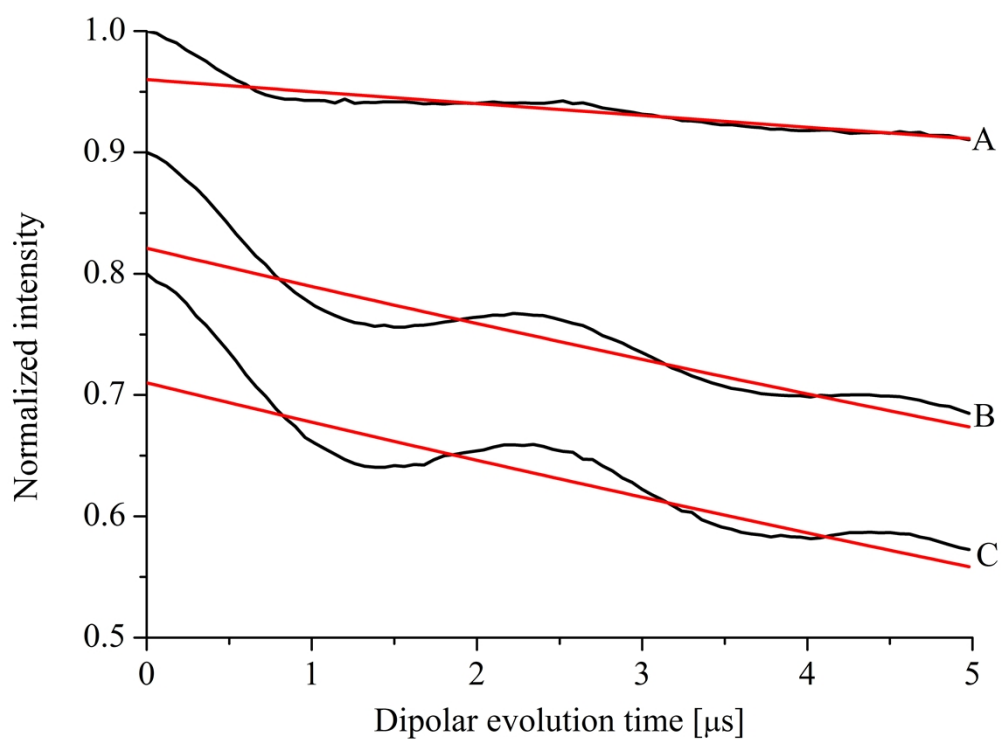


**Fig. S5.** PELDOR time traces obtained at G-band frequencies at a temperature of 25 K (black curves) and the corresponding exponential background functions (red curves). The positions A, B and C correspond to the positions in the spectrum depicted in Fig. 4.

## 6. Fitting of the G-band PELDOR time traces using the PELDOR database

Simulation of the full set of the G-band PELDOR time traces was performed with the PELDOR database approach.<sup>33</sup> For the creation of the PELDOR database three cartesian coordinate systems  $\{x_1, y_1, z_1\}$ ,  $\{x_2, y_2, z_2\}$  and  $\{x, y, z\}$  were defined. The coordinate systems  $\{x_1, y_1, z_1\}$  and  $\{x_2, y_2, z_2\}$  correspond to the trityl g-tensor frame (Fig. S6). The  $z_1$  and  $z_2$  - axes are collinear to the pseudo- $C_3$  symmetry axis of the trityl moieties. The  $x_1$  and  $x_2$  - axes are chosen collinear to the  $\sigma$ -bonds of the central trityl carbon atoms that are aligned along the linker axis. The  $y_1$  and  $y_2$  - axes are orthogonal to the  $x_1$  and  $x_2$  - axes, respectively. The third, reference coordinate system  $\{x, y, z\}$ , that is associated with the biradical linker, is held constant (Fig. S7). The  $z$ -axis of the reference frame is aligned along the mean linker axis, and the  $x$ -axis is aligned orthogonally to the plane, containing two axes  $z_1$  and  $z$ . The coordinate systems  $\{x_1, y_1, z_1\}$  and  $\{x_2, y_2, z_2\}$  rotate with respect to this reference frame and the orientations of  $\{x_1, y_1, z_1\}$  and  $\{x_2, y_2, z_2\}$  with respect to  $\{x, y, z\}$  are described by the Euler angles  $\{\alpha_1, \beta_1, \gamma_1\}$  and  $\{\alpha_2, \beta_2, \gamma_2\}$  in  $ZXZ$ -convention shown in Fig. S6.

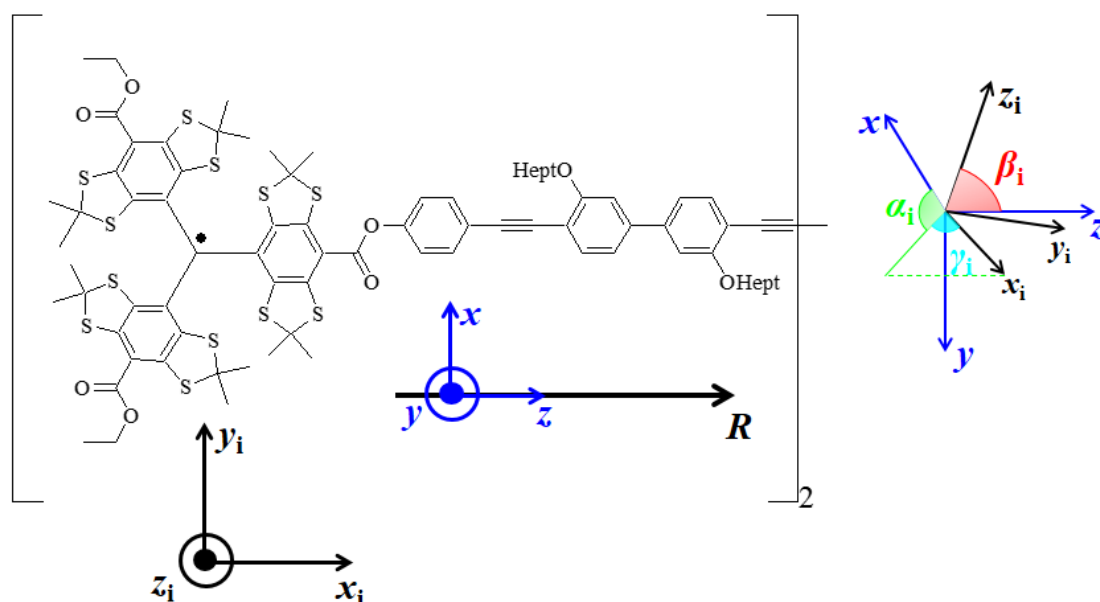


**Fig. S6.** **Left.** Schematic representation of the trityl moiety g-tensor frame  $\{x_i, y_i, z_i\}$  with the fixed reference frame  $\{x, y, z\}$  **Right.** Euler angles  $\{\alpha_i, \beta_i, \gamma_i\}$ , describing the rotation of the trityl g-tensor frame with respect to the fixed reference frame.

The Euler angle  $\alpha_i$  is the angle between the line of nodes  $N_i$  (the intersection line of the planes  $x_i$ - $y_i$  and  $x$ - $y$ ) and the  $x$  axis. According to our definition, the angle  $\alpha_1$  is equal to zero for all biradicals. The  $\beta_i$  is the angle between the trityl g-tensor frame  $z_i$ -axis and the reference frame  $z$ -axis. In the simplified schematic representation depicted in Fig. S6 (left) the  $\beta_i$  angle equals to  $\pi/2$ . The  $\gamma_i$  is the angle between the line of nodes  $N_i$  and trityl  $x_i$ -axis. This angle describes the rotation of the trityl moiety around the g-tensor frame  $z_i$ -axis. Due to the invariance of the PELDOR signal with respect to a permutation of the two identical radicals, the Euler angles have only to be varied in a restricted angle parameter space:  $(\alpha_1 = 0, 0 \leq \beta_1 \leq \pi/2, 0 \leq \gamma_1 < \pi)$  and  $(0 \leq \alpha_2 < \pi, 0 \leq \beta_2 \leq \pi/2, 0 \leq \gamma_2 < \pi)$  in order to generate PELDOR time traces of all possible forms. Within this 5-dimensional angle parameter space, a set of 172800

PELDOR time traces  $S_i$  were calculated for each interspin distance  $R$  with a resolution of  $10^\circ$  for  $\beta_1$  and  $\beta_2$  angles and  $15^\circ$  for the angles  $\gamma_1$ ,  $\gamma_2$  and  $\alpha_2$ . These calculated PELDOR time traces, which constitute the elements of the PELDOR database, were compared to the set of the experimental time traces. In order to account for possible modulation depths inaccuracies in the simulated PELDOR time traces, caused either by incorrectly adjusted pump and detection pulse lengths or by uncertainties in the calculation of the excitation profile of the pulses, the value given by expression (2) was minimised:

$$\left\| (1 - S_{exp}) - f(1 - S_i) \right\|_{f,i}^2 \rightarrow \min \quad (2)$$

The procedure was performed with respect to the parameter  $f$  within the range ( $0.8 < f < 1.2$ ) and parameter  $i$  which denotes the number of the spin label conformer.  $S_i$  and  $S_{exp}$  represent computed and experimental signals, respectively. The procedure (2) yielded numbers  $i_1$  and  $f_1$ . In the next step the fit of the experimental traces was improved further by minimising the value given by (3)

$$\left\| (1 - S_{exp}) - f \left( 1 - \frac{S_{i_1} + S_i}{2} \right) \right\|_{f,i}^2 \rightarrow \min \quad (3)$$

with respect to  $i$  and  $f$ . This gives the conformer number  $i_2$ . The procedure was iteratively repeated 50 times, yielding each time a set of Euler angles of  $(\beta_1, \gamma_1, \beta_2, \gamma_2, \alpha_2)$  and a distance  $R$ . Note, that a dataset from the PELDOR database can be chosen several times, thereby increasing its statistical weight.

Two types of simulations using the concept of the PELDOR database were performed. In the first approach a *model free* search of the conformations has been incorporated, using the full database of the PELDOR signals. In the second approach additional constrains on the selection of the conformations have been imposed in order to reflect the free rotation of the linker segments.

The fitted PELDOR time traces and distance distribution function obtained with the *model-free* approach are depicted in Fig. S7 (Top). The main peak at 4.9 nm and the shape of the distance distribution function are in a good agreement with the result of Tikhonov regularization analysis of the DQC, SIFTER and PELDOR data. However, the *model-free* fitting procedure did not yield uniform distribution of the Euler angle  $\alpha_2$  (see Fig. S7 bottom left). The Euler angle  $\alpha_2$  is defined as the angle between the plane containing the vectors  $z$  and  $z_1$  and the plane containing vectors  $z$  and  $z_2$ . For biradical **1** it is expected that this angle is uniformly distributed from  $0^\circ$  to  $360^\circ$  due to the free rotation of the linker segments.<sup>6</sup>

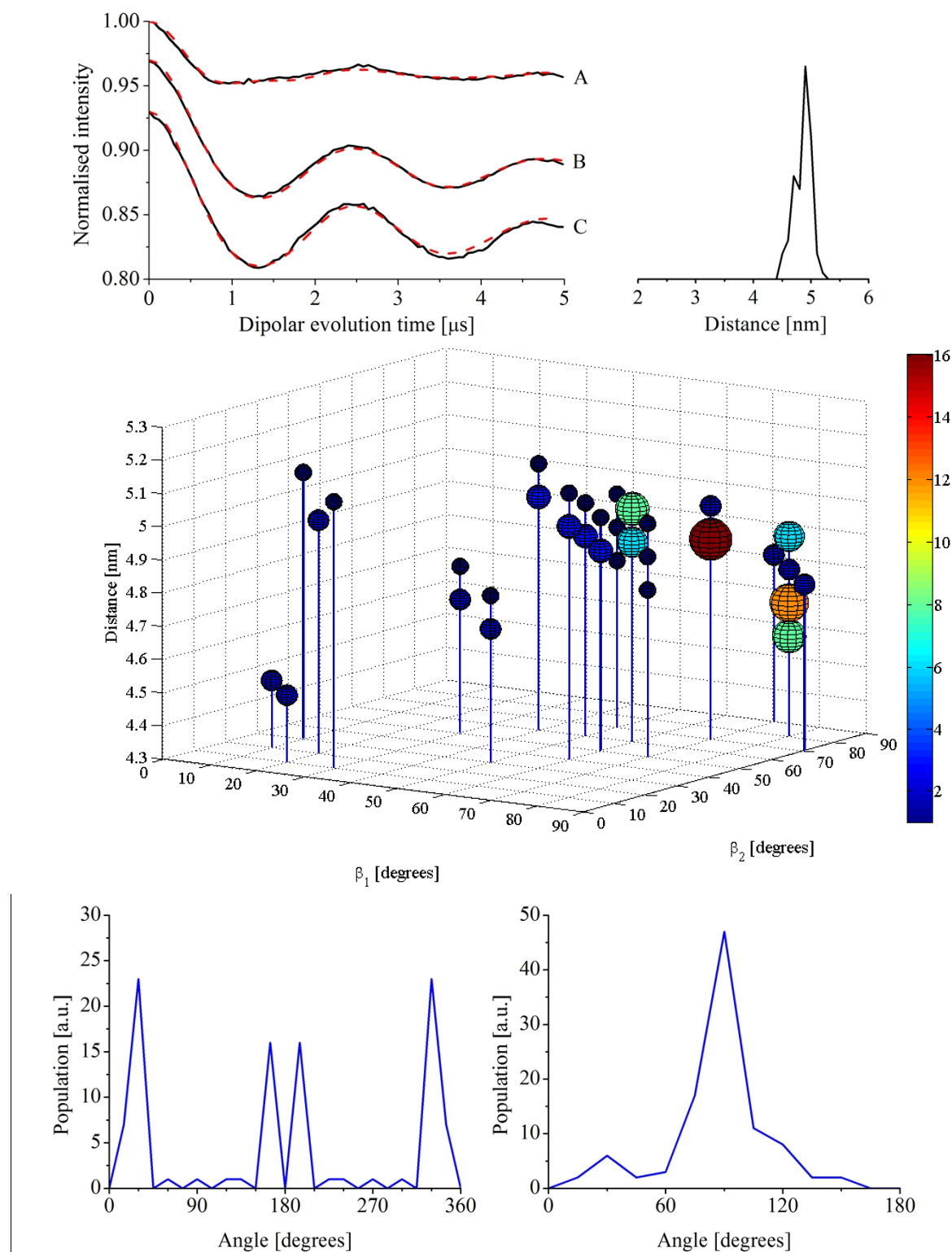


**Fig. S7. Top.** Left-side - Background-divided PELDOR time traces of biradical **1** obtained at G-band frequencies. Solid lines are experimental data, dashed lines are the fits obtained with the first PELDOR database approach (*model-free* approach). Positions A, B and C correspond to the positions in the G-band spectrum depicted in Fig. 4. Right-side - Distance distribution function obtained from the PELDOR database *model-free* fit approach.

**Middle.** Set of the biradical **1** conformers, characterised with the angles  $\beta_1$ ,  $\beta_2$  and a distance  $R$ , obtained with the PELDOR database *model-free* approach. The colour code and size of the balls represent the statistical weights of the distinct conformer.

**Bottom.** Corresponding set of the biradical **1** conformers, characterised with the  $\alpha_2$  angles (left-side) and  $\gamma_i$  angles (right-side). Axes of ordinates correspond to the statistical weight of the conformers.

In the second fitting approach, the PELDOR database was averaged over this angle  $\alpha_2$  leading to a smaller signal database that contains only 14400 signals for various Euler angles ( $\beta_1, \gamma_1, \beta_2, \gamma_2$ ).

The fitted PELDOR time traces, distance distribution function and a set of the biradical **1** conformers with their statistical weights are depicted in Fig. S8. In this approach a good fit of the experimental PELDOR signals was achieved as well. However, the statistical weight of the relative spin label orientations and distance distribution function differ from the result obtained in the first, *model-free* approach. This led to the conclusion, that a set of the three G-band PELDOR time traces with their weak spectral anisotropy is not enough to gain information about the trityl biradical conformational flexibility unambiguously.

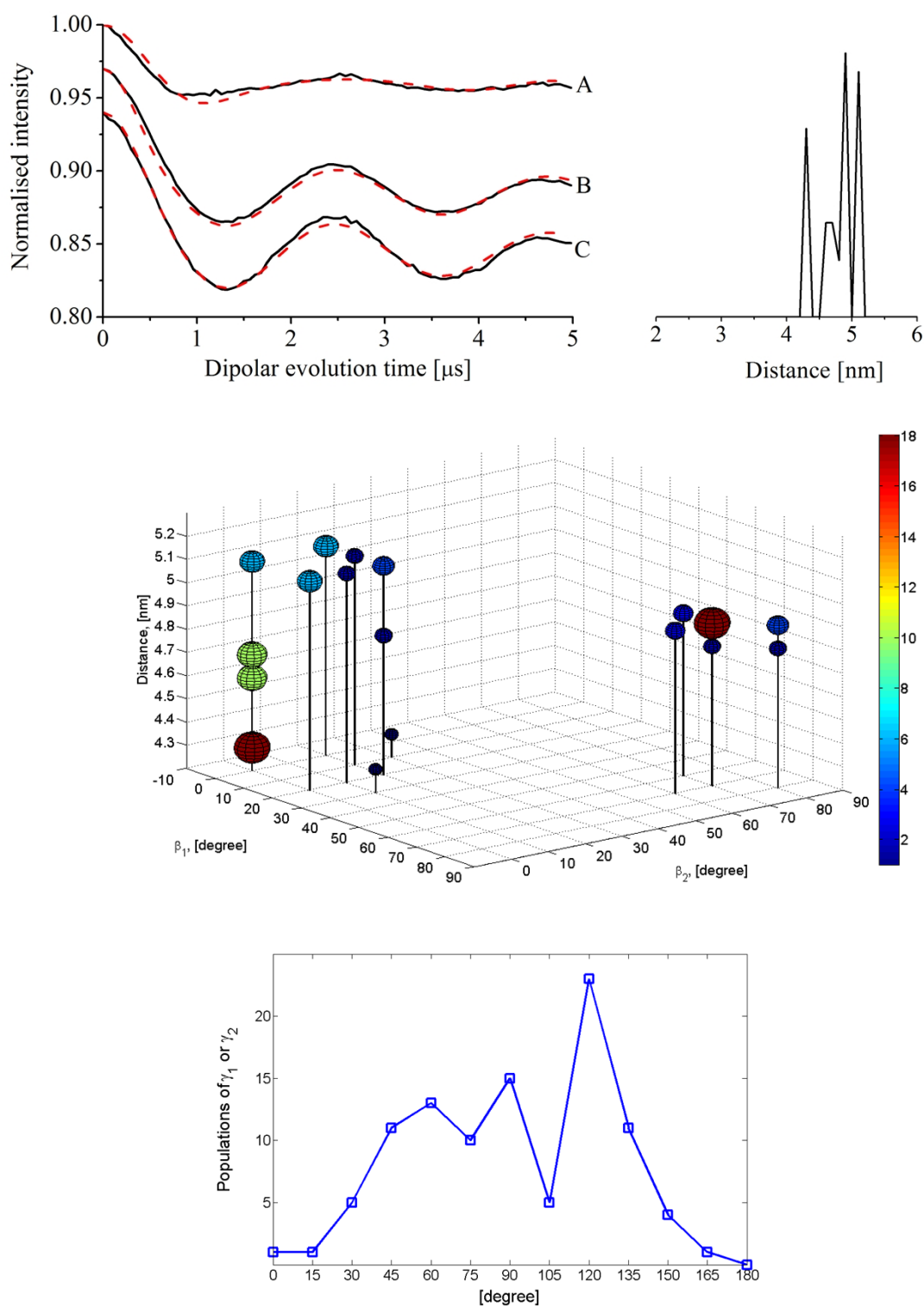


**Fig. S8. Top.** Left-side - Background-divided PELDOR time traces of biradical **1** obtained at G-band frequencies. Solid lines are experimental data, dashed lines are the fits obtained with the second PELDOR database fit approach. Positions A, B and C correspond to the positions in the G-band spectrum depicted in Fig. 4. Right-side - Distance distribution function obtained from the second PELDOR database fit approach.

**Middle.** Set of the biradical **1** conformers, characterised with the angles  $\beta_1$ ,  $\beta_2$  and a distance  $R$ , obtained with the second PELDOR database approach. The colour code and size of the balls represent the statistical weights of the distinct conformer.

**Bottom.** Corresponding set of the biradical **1** conformers, characterised with  $\gamma_i$  angle. Axes of ordinates correspond to the statistical weight of the conformers.

## 7. References

- S1 S. Stoll and A. Schweiger, *J. Magn. Reson.*, 2006, **178**, 42.
- S2 M. K. Bowman, C. Mailer and H. J. Halpern, *J. Magn. Reson.*, 2005, **172**, 254.